Fire Safety Journal 79 (2016) 44–56

Contents lists available at ScienceDirect

Fire Safety Journal

journal homepage: www.elsevier.com/locate/firesaf

Numerical simulation of surface forest fire in Brazilian Amazon

Paulo Bufacchi [a,*], Guenther C. Krieger [a], William Mell [b], Ernesto Alvarado [c], José Carlos Santos [d], João Andrade Carvalho Jr. [e]

[a] Department of Mechanical Engineering, Escola Politécnica da Universidade de São Paulo, Cidade Universitária, São Paulo, SP, Brazil
[b] U.S. Forest Service Pacific Northwest Research Station, Pacific Wildland Fire Sciences Lab, Seattle, WA, USA
[c] Pacific Wildland Fire Sciences Laboratory, School of Forest Resources, University of Washington, Seattle, WA, USA
[d] Instituto Nacional de Pesquisas Espaciais-INPE, Cachoeira Paulista, SP, Brazil
[e] Universidade Estadual Paulista – UNESP, Guaratinguetá, SP, Brazil

ARTICLE INFO

Article history:
Received 24 October 2014
Received in revised form
12 October 2015
Accepted 29 November 2015
Available online 8 December 2015

Keywords:
Surface fire
Numerical simulation
Turbulent combustion
Brazilian Amazon
Rate of spread

ABSTRACT

This paper investigates fire spread through surface fuels of the Brazilian Amazon by using a three-dimensional, fully transient, physics-based computer simulation approach. Computer simulations are obtained through the solution to governing equations of fluid dynamics, combustion, heat transfer and thermal degradation of the vegetative fuel. Surface fuel fires composed mostly of dead leaves and twigs were numerically simulated and the calculated rate of spread was compared to findings from field observations. The importance of air humidity, vegetation temperature, moisture content, surface to volume ratio and bulk density was evaluated through the variation of each one individually in numerical simulation runs. Conclusions show that in the range of parameter variation considered, the most important parameters are the vegetation moisture, surface area to volume ratio, and bulk density. The vegetation initial temperature and air humidity, in the range of variation studied, did not influence the fire rate of spread. The numerical simulations also showed that the radiation process is very important and directly affects the fire rate of spread. Convection is less important because of the absence of external wind. The model is able to capture the main effects of a surface forest fire typical of the Amazon, and can be used as a numerical tool for studying such fires.

© 2015 Elsevier Ltd. All rights reserved.

1. Introduction

Many field and laboratory experiments and numerical simulations for the prediction of the rate of spread (ROS) of wildland fires have been run worldwide. These efforts, however, concentrate on ecosystems that are very different from those found in the Amazon. The closest fire systems studied were Mediterranean shrubs and grasslands, which have been experimentally studied by Santoni et al. [1] and Morandini et al. [2] and numerically by Morvan and Dupuy [3], Mell et al. [4] and Morvan et al. [5]. Numerically, the model ranged from simple geometrical models [6] to very complex ones [7–9]. A review of the literature showed an almost total absence of field and laboratory data on surface fire propagation in the Brazilian Amazon. As for numerical simulations, the subject has never been addressed.

It is very difficult, if not prohibitive, to study forest fires in large-scale repeatable field experiments, because of cost and safety implications and the adverse effects on local vegetation. In order to better understand the combustion processes that occur in forest fires, it is important to know the characteristics of vegetative fuels, specifically their chemical composition. This is a challenging problem in itself. Because of the wide variety of plant species and the difference in their chemical composition, average values are used to generically describe the vegetative material.

Excluding burns in already deforested areas, the most important fire in the Amazon ecosystem is surface fire, which is characterized by the burning of dead and undergrowth vegetation, such as herbs, layer of leaves and branches. These fires do not cause significant damage to large trees, but are extremely harmful to young plants and lower vegetation, mainly for forest regeneration [10].

Burning of tropical evergreen rainforests alters forest composition and structure. Common tree species suffer the greatest total mortality. Even 15 years after burning, forests show no evidence of regaining lost species. Prospects for species recovery are diminished because surface fires reduce seed availability by 85% in the litter layer and 60% in the upper 1.5 cm of soil, while flowering and fruiting of trees in and near burned forests also decreases. Recurrent fires rapidly reduce the size and density of surviving

* Correspondence to: Rua Dr. Thirso Martins, 200/62, 04120-050 São Paulo, SP, Brazil.
E-mail address: paulo_bufacchi@hotmail.com (P. Bufacchi).

http://dx.doi.org/10.1016/j.firesaf.2015.11.014
0379-7112/© 2015 Elsevier Ltd. All rights reserved.

unburned forest fragments and kill regenerating vegetation, further depleting the prospects for recovery of mature forest species. Fires in tropical forests frequently occur in surface fuels, so understanding the characteristics and compositions of litter systems will be essential for predicting burning characteristics. Litter arrangement, loading, moisture content, type and composition are all important modifiers of fire behavior. Furthermore, litter from different species has large variations in energy values and flammability. Therefore, the phytosociological mix of litter-generating species can influence the flammability, sustainability, spread and heat-release characteristics of fires. The majority of tropical fires, however, are neither fast-spreading nor intense. They are severe nevertheless because the impact to the forest is quite large. Fires in tropical rainforests range from easily-extinguished litter fires to nearly impossible-to-extinguish ground fires. In recurrent wildfires, average fire intensities are ten times greater (30 versus 307 kW m^{-1}) and can spread twice as fast (0.25 versus 0.52 m min^{-1}). Closed-canopy forests are protected from the wind, and fire intensities and spread rates in such forests are also kept low by the high moisture content of fuels. However, even at low intensities, slow-moving fires are severe because of the mortality caused by the long fire-contact times and the resultant heat transfer at the base of trees [11].

The objective of this work is the prediction of a surface fire rate of spread in the Brazilian Amazon ecosystem and the determination of the most important parameters affecting the fire rate of spread. For the numerical simulation, we have used the physics-based model WFDS (Wildland-Urban Fire Dynamics Simulator), which is based on conservation equations governing fluid mechanics, combustion and heat transfer.

2. Field observations

Simulated rates of spread were compared to field surface fire observations in the States of Acre and Mato Grosso in the Brazilian Amazon (Fig. 1).

Field observations are not part of this work, but a brief description is made in this section for reference because their results are used for comparison with the numerical simulations presented in this paper.

Crude by design field observations were conducted in the cities of Cruzeiro do Sul (State of Acre) and Alta Floresta (State of Mato Grosso). These field observations were conducted by a team that performs similar observations regularly in the same region. These two field observations were not designed to fulfill the comparison needs with the numerical model (WFDS), but they are useful in that they provide a first comparison for WFDS results.

In Cruzeiro do Sul, a set of field observations was carried out near the fire site where a research group performed Amazon deforestation fire studies. The litter material in the adjacent area of the main burning experiment was collected and transported to a nearby farm. In this farm, the litter was spread in a grass field for drying. In a nearby location, the soil was cleaned and worked for parallelism and flatness. A set of small iron sticks marked a central point and a 1.5 m circumference around it. Litter was then collected, weighted and spread inside the marked circumference. Then litter load, humidity, and temperature were all measured prior to ignition. Wind speed and condensed phase temperature were also measured prior to fire propagation. Temperature was checked by an infrared measurement system and humidity by a Thermo-Technik device. Wind speed was measured by an anemometer, and its direction determined. Ignition took place in the center of the circumference by means of small amount of ethanol poured inside a 10 cm round area.

In each of the observation areas in the Alta Floresta site, a 50×50 cm^2 area was selected to quantify the corresponding litter biomass. The material was weighed with a spring scale. The depth of the litter layer was determined with a steel ruler. Litter moisture content was determined in the laboratory by collecting biomass samples in the 50×50 cm^2 area and letting them dry at 85 °C until no weight loss was observed. Air temperature and humidity were determined with a specific sensor (portable Vaisala Humicap). Air wind speed was not measured, but it is judged to be negligible, since no leaves movement was observed. Other field wind measurements conducted inside the forest confirmed this assumption

Fig. 1. Location of field observations. Site A is located in the city of Cruzeiro do Sul in the State of Acre, while site B is located in the city of Alta Floresta in the State of Mato Grosso.

Table 1
Input values for the numerical simulation from field observations in the States of Acre (AC) and Mato Grosso (MT) litter.

Symbol	Simulation for field observation #1-AC	Simulation for field observation #4-AC	Simulation for field observation #6-AC	Simulation for field observation #8-AC	Simulation for field observation #1-MT	Simulation for field observation #3-MT	Simulation for field observation #4-MT
Gas phase							
Δh_c (kJkg^{-1})	17,700	17,700	17,700	17,700	17,700	17,700	17,700
	0.35	0.35	0.35	0.35	0.35	0.35	0.35
χ_s	0.01	0.01	0.01	0.01	0.01	0.01	0.01
T (°C)	33.7	30.3	32.0	27.0	34.1	30.0	30.9
Humidity (%)	47.0	51.0	60.0	60.0	27.0	34.5	36.0
Solid phase							
σ (m^{-1})	4,000	4000	4000	4000	4000	4000	4000
χ residue	0.10	0.15	0.19	0.18	0.31	0.28	0.38
$r = r_0 \exp(E_g/2k_BT)$ (kg m^{-3})	11.9	13.4	12.6	11.0	9.2	11.9	9.0
$c_{p,v}$ (kJkg^{-1}K^{-1})	=0.1+0.0037 Ts	=0.1+0.0037 Ts	=0.1+0.0037 Ts	=0.1+0.0037 Ts	=0.1+0.0037 Ts	=0.1+0.0037 Ts	=0.1+0.0037 Ts
ρ_e (kg m^{-3})	650	650	650	650	650	650	650
ρ_{bv} (kg m^{-3})	13.18	15.70	15.49	13.44	13.34	16.45	14.49
Ts (°C)	33.7	30.3	32.0	27.0	34.1	30.0	30.9
M (%)	10.0	22.0	13.0	16.0	14.4	13.9	16.4
Litter depth (m)	0.12	0.12	0.09	0.06	0.05	0.05	0.05

[12].

3. Overview of the numerical model

The numerical approach used is WFDS (version 6.0 rev. 9977; [13]), which is an extension of the capabilities of FDS (Fire Dynamics Simulator) to model outdoor fire spread and smoke transport problems that include vegetative and structural fuels and complex terrain [9]. WFDS is developed by the U.S. Forest Service in collaboration with the National Institute of Standards and Technology (NIST), also in the United States. FDS is a structure (buildings) fire behavior model developed by NIST (www.nist.gov) in cooperation with VTT Technical Research Center of Finland, industry and academics. The methods of computational fluid dynamics (CFD) are used to solve the three-dimensional time-dependent equations governing fluid motion, turbulent combustion, and heat transfer. The numerical model is based on the large-eddy simulation (LES) approach and provides a time-dependent, coarse-grained, numerical solution to the governing transport equations for mass, momentum, and energy.

The effect of thermal expansion because of chemical reaction and heat and mass transfer enters the computation through an elliptic constraint, derived using the energy equation, on the velocity field. The local mean temperature is then obtained via the ideal gas equation of state. Dissipation of kinetic energy is achieved through a simple closure for the turbulent stress: the constant coefficient Deardorff model [14]. The turbulent transport of heat and mass is accounted for by use of constant turbulent Prandtl and Schmidt numbers, respectively. The subgrid heterogeneity of species concentrations and temperature is treated in conjunction with the reaction, heat transfer, and radiation intensity models. The continuity equation is solved together with the Stokes form of the momentum equations on a structured Cartesian staggered grid. The spatial discretizations are second-order accurate for uniform grids. Species mass equations are advanced using a modified version of MacCormack's predictor–corrector scheme [15] and the momentum equations are advanced using a two-stage projection scheme based on the explicit modified Euler method. Turbulent combustion for the gaseous phase is modeled based on the Eddy Dissipation Concept (EDC) model of Magnussen and Hjertager [16]. The condensed phase model is assumed to be composed of fixed, thermally thin (temperature can be assumed to be uniform throughout the fuel element), optically black, fuel elements. More than one type of thermally thin element can be represented. The thermally thin assumption is commonly used in fire spread models involving fine wildland fuels, such as grass and foliage of shrubs and trees [17]. Both convective and radiative heat transfer between the gas phase and the vegetation are accounted for, as is the drag of the vegetation on the airflow. In general, as the temperature of a vegetative fuel increases, first moisture content is removed, followed by pyrolysis-the generation of fuel vapors. In the modeling approach used here, the temperature equation for the fuel bed is solved with a two-stage process: endothermic water evaporation and vegetation pyrolysis.

4. Simulation inputs

Computer simulations for field burn observations in the States of Acre and Mato Grosso were conducted. Validation checks of the numerical simulation were made by comparing time histories of the predicted and measured ROS. ROS is an important fire variable. It is the result of the coupled processes of heat generated by gas-phase combustion, convective and radiative heat transfer to the vegetation, heat transfer within the fuel bed, and the resulting thermal degradation of the vegetation, which supplies fuel to sustain the combustion process.

The numerical model requires a number of thermo-physical properties for the gas phase and the vegetative fuel, as listed in Table 1 and described as follows.

(1) Density: A value of ρ_e=650kgm^{-3} was used for the fuel element density, which corresponds to a fresh jackfruit leaf as measured by Jayalakshmy and Philip [18]. The jackfruit genus belongs to the Moraceae botanical family, which comprises 75 genera and 1550 species, most of them found in tropical regions. In Brazil, there are 28 genera and 340 species.
(2) Initial temperature: The initial temperature of the litter is indicated in Table 1.

(3) Moisture content: The moisture content, *M*, determined on a dry basis, is given as a percentage

$$M = \frac{m_{e,wet} - m_{e,v}}{m_{e,v}} \times 100\% \quad (1)$$

where $m_{e,wet}$ is the measured mass of the virgin vegetation and $m_{e,v}$ is the mass of the dried virgin vegetation; the subscript e denotes a vegetative fuel element of a given type. Moisture content values are shown in Table 1.

(2) Residue fraction: Residue fraction values are presented in Table 1 and were calculated according to the equation $\chi_{residue}=\frac{m_{e,residue}}{m_{e,v}}$, where $m_{e,residue}$ is the mass of residue (leaves char and unburned twigs) for the fuel element e.

(3) Specific heat: The relation for the specific heat of dry virgin vegetation is as coded in WFDS and shown in Table 1.

(4) Surface-to-volume ratio: The surface to volume ratio is 4000 m^{-1} that considers in average a leaf length of 125 mm, width of 80 mm and thickness of 0.5 mm.

(5) Heat of combustion: Δh_c=17, 700 kJ kg^{-1} is the heat released per kg of gaseous fuel and not per kg of vegetative fuel. It was used the value reported by Mell et al. [9], as the heat of combustion does not vary enough to be significant in the numerical evaluation of the fire [19].

(6) Geometry: The computer model represents the litter as a rectangular volume. The litter depth varies as shown in Table 1.

(7) Bulk density: The model equations require the bulk density of the dry (zero moisture) thermally thin vegetation. An estimate for the bulk density of the dry thermally thin vegetation can be obtained from the experimentally measured loss of dry mass Δm_{dry}, and an estimated volume of the litter, $\rho_{bv}=\Delta m_{dry}/V_{litter}$. In all cases, the vegetation is assumed to be distributed uniformly throughout the rectangular volume so that the bulk density is spatially independent. The litter bulk density varies depending on the field location, as reported on Table 1.

(8) Packing ratio: The packing ratio $\beta = \rho_{bv}/\rho_e$ is an important parameter in the drag and convective and radiative heat transfer. Its value depends on the bulk density, ρ_{bv}, and the fuel element density, ρ_e.

(9) Radiative fraction: The radiative fraction, χ_r, is a useful quantity in fire science. It is the nominal fraction of the combustion energy that is emitted as thermal radiation. For most combustibles, χ_r is between 0.3 and 0.4 [20].

5. Results and discussion

The sensitivity of the model predictions for the rate of spread on grid resolution was tested. The computational domain size was 1 m × 1 m × 0.5 m in *xyz* directions with *z* vertical (see Fig. 2). As the flame height in the field observations was around 0.3 m, the domain height of 0.5 m was found to be enough to represent well all the processes involved.

Any numerical simulation of fluid mechanics must verify whether the results are mesh independent. The process of discretizing the transport equations generates errors that are proportional to the size of the mesh cell. In addition, in fire simulations the literature [8,20] recommends the evaluation of two parameters that guide the mesh size.

A parameter used for simulations involving pool fires (similar in characteristics to the early stages of the fire studied in this paper), which is a measure of how well the flow field is resolved, is given by the non-dimensional relation $D^*/\delta x$, where D^* is the characteristic diameter of the fire

$$D^* = \left(\frac{Q}{\rho_\infty c_p T_\infty \sqrt{g}} \right)^{\frac{2}{5}} \quad (2)$$

The smaller the characteristic fire diameter, the smaller the size of the cells in order to properly resolve the fluid flow and the dynamics of the fire. The parameter δx is the nominal size of a mesh cell. The value of $D^*/\delta x$ ranges from 4 (coarse meshes) to 16 (fine meshes) [20]. The quantity $\dot{Q}$ is the rate of heat release of the fire. The average value of the heat release rate was used in this paper to determine the characteristic fire diameter value. The surface fire behaves like a pool fire up to a distance of approximately 40 cm from the fire ignition location. Even though an average value is used for the rate of heat release of the fire, this does not compromise the numerical simulation outcomes, as a mesh sensitivity analysis is performed and this ultimately guarantees that the results are mesh independent. The quantity $D^*/\delta x$ can be thought of as the number of computational cells that span the characteristic fire diameter. The accuracy of the calculation increases with the number of cells. It is useful to assess the quality of the mesh in terms of this dimensionless parameter instead of an absolute cell size. For example, a cell size of 10 cm may be suitable for evaluating the spread of smoke throughout a fire of considerable size, but may not be suitable for studying a small fire. Table 2 shows the values for the cell sizes in each simulation according to the expression for D^*.

The second parameter defines how small the mesh cell needs to be in order to resolve the combustion zone and heat transfer gradients. Morvan and Dupuy [8] use a rule based on optical length. This empirical rule provides a length scale representative of the heat transfer by radiation to determine the number of cells that represents the vegetation and is given by

$$\delta_r = \frac{4}{\beta \sigma_e} \quad (3)$$

where δ_r is the optical length. It was considered that to properly represent the processes involved with the vegetation, at least three cells must be within the above-defined optical length. Table 3 shows the optical length for each simulation and the maximum size of the cell (equivalent to one third of the optical length).

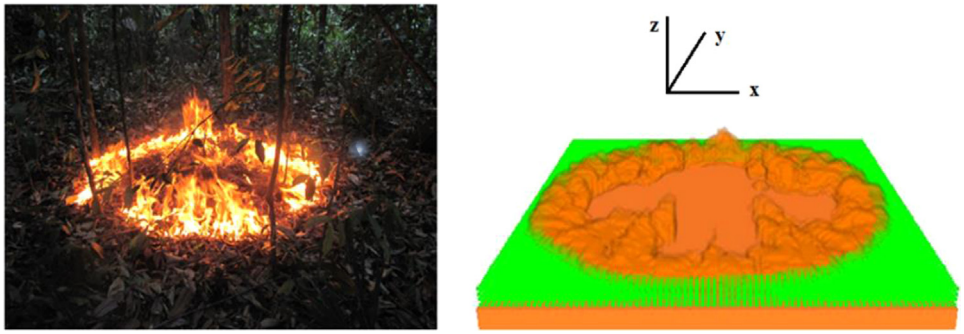

Fig. 2. Surface fire observation in the State of Mato Grosso, showing the fire propagation in its early stages (left). WFDS simulation of the surface fire (right).

Table 2
Evaluation of mesh size in terms of D^* for the field observations of Cruzeiro do Sul (AC) and Alta Floresta (MT).

Field observation #	Coarse mesh (cm)	Moderate mesh (cm)	Fine mesh (cm)
1 – AC	8.62	3.45	2.15
4 – AC	6.57	2.63	1.64
6 – AC	7.30	2.92	1.82
8 – AC	4.70	1.88	1.17
1 – MT	6.39	2.56	1.60
3 – MT	7.10	2.84	1.78
4 – MT	6.03	2.41	1.51

Table 3
Optical length and maximum cell size for the simulations of the field observations of Cruzeiro do Sul (AC) and Alta Floresta (MT).

Field observation #	Optical length (cm)	Maximum cell size (cm)
1 – AC	4.9	1.6
4 – AC	4.1	1.4
6 – AC	4.2	1.4
8 – AC	4.8	1.6
1 – MT	4.9	1.6
3 – MT	4.0	1.3
4 – MT	4.5	1.5

Table 4
Mesh sensitivity study for field observations #1 and #3 of Alta Floresta (MT).

Field observation #	Cell size – *xyz* (cm)	Difference in ROS from finest mesh resolution (%)
1	$2.5 \times 2.5 \times 2.5$	+71
1	$1.25 \times 1.25 \times 1.25$	0
1	$1.0 \times 1.0 \times 1.0$	0
1	$0.625 \times 0.625 \times 0.625$	Finest mesh
3	$2.5 \times 2.5 \times 2.5$	+75
3	$1.25 \times 1.25 \times 1.25$	0
3	$0.625 \times 0.625 \times 0.625$	Finest mesh

As a next step, the mesh independence is assessed. Mesh sensitivity study is the most important assessment to be done, and it was performed for field observations #1 and #3 of Mato Grosso (Table 4). As can be seen, ROS does not vary for cell sizes of 1.25 cm and smaller. Furthermore, cell size of 1.25 cm is in accordance with data in Tables 2 and 3. Thus, considering the three above criteria and the litter depth, the cell size of the computational mesh used for the simulations of the field observations of Alta Floresta (MT) is 1.25 cm and for Cruzeiro do Sul (AC) it is 1.00 cm.

Simulations for the field observations of Alta Floresta (MT) and Cruzeiro do Sul (AC) were performed to verify how well the model can predict the field observation ROS and are presented next.

5.1. *Simulation of the field observations of Alta Floresta (MT)*

A simulated mass loss time history for the entire vegetation in the domain is shown in Fig. 3. Time histories of the predicted radiant and convective heat fluxes in a grid cell located along the litter's surface 35 cm from its center are shown in Figs. 4 and 5 respectively.

The initial dry mass, final mass and percentage of final mass to the initial dry mass are as shown in Table 5. The ratio of final mass to initial dry mass represents the total initial dry mass that was not burned in the simulation after 180 s. The mass loss curve simulated for field observation #4 has a slightly different shape when compared to simulations of field observations #1 and #3, because of the fact that there is comparatively greater dry mass that has not been burned after 180 s. This indicates that ROS calculated by numerical simulation for this field observation is smaller than the others, as can be seen in Table 6. In these field observations, ROS was taken in four different directions and its minimum and maximum values are shown in Table 6.

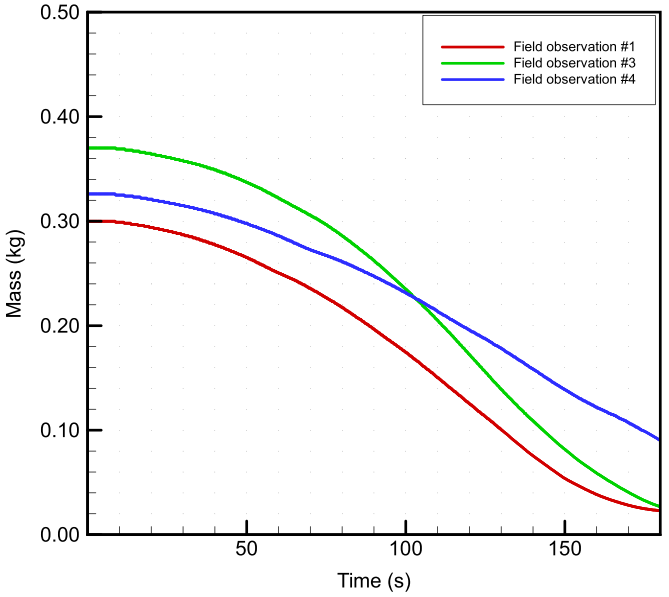

Fig. 3. Mass loss time history curves for each of the three field observations of Alta Floresta (MT).

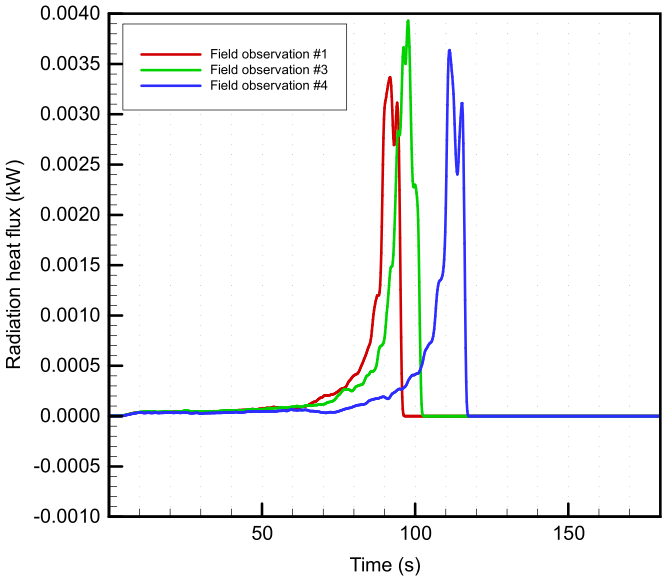

Fig. 4. Time history curves of the predicted radiant heat flux in a grid cell located along the litter's surface 0.35 m from the center of the surface fire for each of the three field observations of Alta Floresta (MT).

It can be seen from Figs. 4 and 5 that radiation heat flux is dominant over convection heat flux. After studying other systems, Silvani and Morandini [21] came to the same conclusion. For up to about half of the vegetation moisture content evaporation process in the three cases examined, the net heat flux by radiation is the only method available for heating the fuel element. For the three cases examined, it is observed that the fuel element under analysis provides net energy by convection to the gaseous medium before it starts receiving this type of energy.

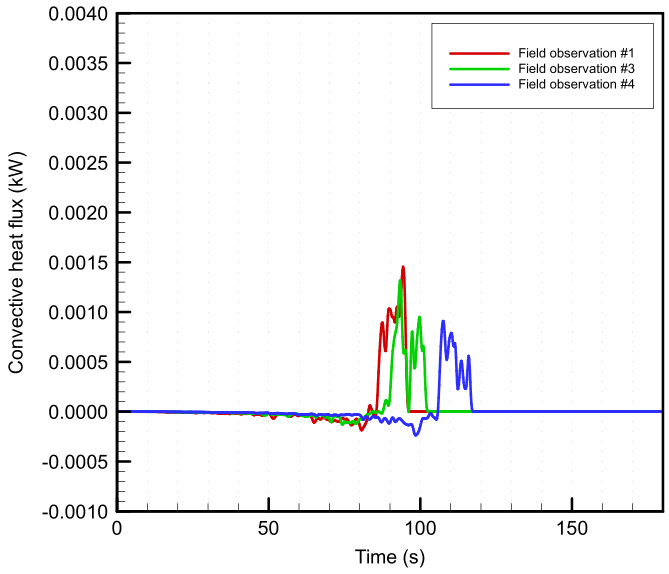

Fig. 5. Time history curves of the predicted convective heat flux in a grid cell located along the litter's surface 0.35 m from the center of the surface fire for each of the three field observations of Alta Floresta (MT).

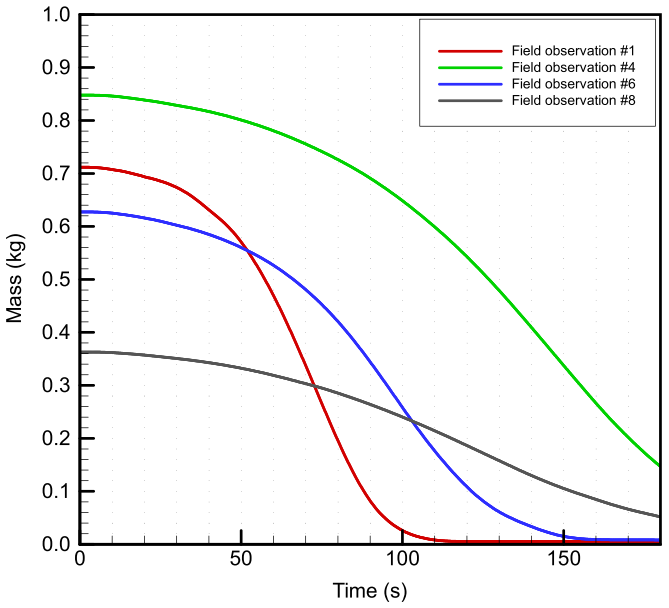

Fig. 6. Mass loss time history curves for each of the four field observations of Cruzeiro do Sul (AC).

Table 5
Values of the initial dry mass, final mass and ratio of final mass to initial dry mass of Alta Floresta (MT).

Field observation #	Litter height (m)	Initial dry mass (kg)	Final mass (kg)	Ratio of final mass to initial dry mass (%)
1	0.05	0.30	0.02	6.7
3	0.05	0.37	0.03	8.1
4	0.05	0.33	0.09	27.3

Table 6
ROS values for the field observations of Alta Floresta (MT).

Field observation #	Field measured ROS-min (m min^{-1})	Field measured ROS-max (m min^{-1})	Simulated ROS (m min^{-1})
1	0.17	0.28	0.21
3	0.24	0.44	0.20
4	0.19	0.30	0.18

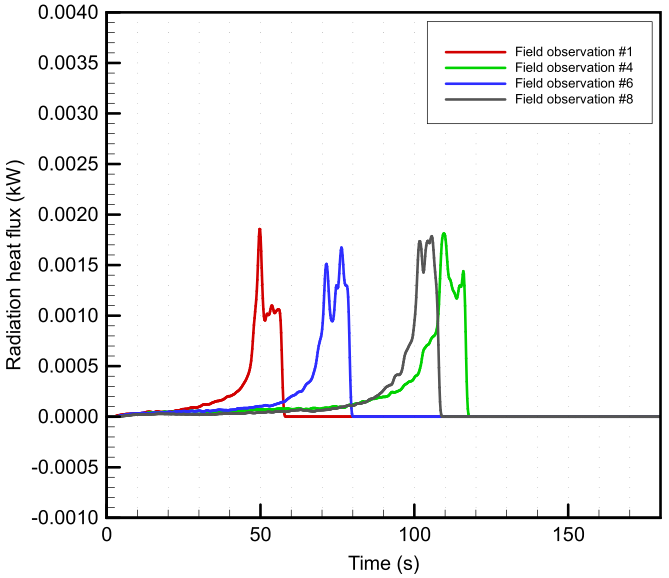

Fig. 7. Time history curves of the predicted radiant heat flux in a grid cell located along the litter's surface 0.35 m from the center of the surface fire for each of the three field observations of Cruzeiro do Sul (AC).

5.2. *Simulation of the field observations of Cruzeiro do Sul (AC)*

It is shown in Fig. 6 the simulated mass loss time history for the entire vegetation in the domain. For the grid cell located along the litter's surface 35 cm from its center, it is shown in Figs. 7 and 8 respectively the time histories of the predicted radiant and convective heat fluxes in a.

In Table 7 it is shown the initial dry mass, final mass and percentage of final mass to the initial dry mass. The simulated mass loss curve for field observations #4 and #8 shows that there is, compared with field observations #1 and #6, a higher dry mass that has not been burned after 180 s. The final masses of numerical simulations for field observations #1 and #6 are very small, and it can be considered that the vegetation total mass in each case was completely consumed. Measurements in the field and simulated ROS are as shown in Table 8.

It can be seen from Figs. 7 and 8 that radiation heat flux is dominant over convection heat flux. For the numerical simulations of field observations #4 and #8, the energy from convection is not available for the fuel element under consideration during moisture content evaporation. In the case of numerical simulations in field observations #1 and #6, for up to half of the vegetation moisture content evaporation process, the net heat flux by radiation is the only method available for heating the fuel element. Similarly to Mato Grosso field observations, the fuel element under analysis provides net energy by convection to the gaseous medium before it receives this type of energy.

As can be seen from Tables 6 and 8, most of the results from the numerical simulation are in the range measured in field observations or very close to them. The reasons for these deviations can be various, including the non-homogeneity in the field observation, measurement errors, number of field measurements and limitations of the numerical model.

To better understand fire behavior and to assess the influence of some input parameters to WFDS, it was performed a qualitative comparison. Taking field observation #1 of Alta Floresta (MT) as a

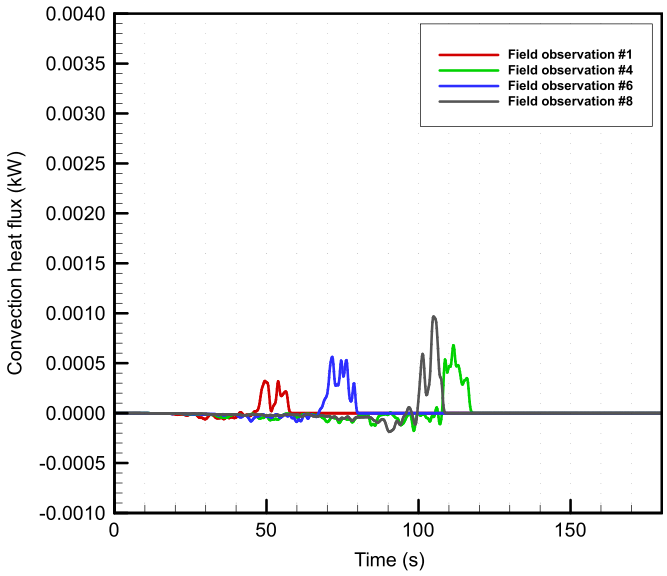

Fig. 8. Time history curves of the predicted convective heat flux in a grid cell located along the litter's surface 0.35 m from the center of the surface fire for each of the three field observations of Cruzeiro do Sul (AC).

Table 7
Values of the initial dry mass, final mass and ratio of final mass to initial dry mass of Cruzeiro do Sul (AC).

Field observation #	Litter height (m)	Initial dry mass (kg)	Final mass (kg)	Ratio of final mass to initial dry mass (%)
1	0.12	0.71	0.005	0.7
4	0.12	0.85	0.150	17.6
6	0.09	0.63	0.008	1.3
8	0.06	0.36	0.050	13.9

Table 8
ROS values for the field observations of Cruzeiro do Sul (AC).

Field observation #	Field measured ROS-min (m min^{-1})	Field measured ROS-max (m min^{-1})	Simulated ROS (m min^{-1})
1	0.13	0.22	0.23
4	0.12	0.16	0.14
6	0.12	0.16	0.19
8	0.12	0.17	0.17

reference, we studied the variation in ROS caused by a change of plus and minus ten percent in the parameters of air humidity, vegetation moisture content, vegetation surface area to volume ratio (SAV), and vegetation bulk density. For the vegetation temperature, a variation of plus and minus 5 °C was considered. Although parameter surface area to volume ratio was constant in all simulations, it is included in this assessment.

5.3. Variation in air humidity for field observation #1 of Alta Floresta (MT)

This case is the same as the field observation #1 of Alta Floresta (MT), the only difference being that two additional simulations were performed to evaluate the effect of air humidity variation. The simulations evaluated what would happen if the air humidity was 10% lower and 10% higher. The 10% value was chosen for the studies because the variation is of significant amplitude for each variable. This is the only analysis that does not refer to vegetation. The impact of the variation of air humidity is described as follows. Field measured and simulated ROS for field observation #1 were 0.21 m min^{-1}. For cases where the air humidity is 10% lower and higher than the value measured in field observation #1, calculated ROS is also 0.21 m min^{-1} (Table 9). For this range of variation in air humidity it can be seen that ROS is not affected by this variable. Although the evaporated vegetation moisture content value goes into the equation that describes the gaseous medium species and therefore affects the air humidity, there is no mechanism in WFDS that accounts for air humidity effects in the vegetation moisture content. However, observing Table 1 data for gas phase air humidity and solid phase moisture content for all field observations, it is not clear a correlation between these two variables.

5.4. Variation in vegetation temperature for field observation #1 of Alta Floresta (MT)

In this section two simulations are compared with the base case described in field observation #1. The difference between the simulations is the variation of the initial vegetation temperature. Vegetation temperature, in the range of values tested, does not affect ROS (Table 10). The vegetation temperature ranged from 27 °C to 34.1 °C, a difference of only 7.1 °C. In the numerical model, the vegetation temperature needs to be raised to 100 °C for the moisture content evaporation to begin. As the vegetation temperature difference to the moisture content evaporation temperature is practically the same, the impact on ROS is negligible.

5.5. Variation in vegetation moisture content for field observation #1 of Alta Floresta (MT)

These simulations evaluated what would happen if the vegetation moisture content was 10% lower and 10% higher than actual value measured in field observation #1 of Alta Floresta (MT). For the case in which vegetation moisture content is 10% lower than the value measured in field observation #1, simulated ROS is 0.23 m min^{-1}. For the case in which the variable is 10% higher, simulated ROS is 0.19 m min^{-1} (Table 11). It was observed that the magnitude of variation in ROS is equal in both cases examined, when compared to field observation #1. In the case with lower vegetation moisture content, ROS is 0.02 m min^{-1} greater than the value measured in the field. For the case with higher vegetation moisture, ROS is 0.02 m min^{-1} smaller than the value measured in the field (Table 11).

Table 9
Parametric variation in air humidity for field observation #1.

	Air humidity (%)	ROS (m min^{-1})	Difference between simulated ROS and field observation ROS (m min^{-1})
Field observation #1	27.0	0.21	
Field observation #1 numerical simulation	27.0	0.21	0
Numerical simulation: air humidity 10% lower than field observation #1	24.3	0.21	0
Numerical simulation: air humidity 10% greater than field observation #1	29.7	0.21	0

Table 10
Parametric variation in vegetation temperature for field observation #1.

	Vegetation temperature (°C)	ROS (m min^{-1})	Difference between simulated ROS and field observation ROS (m min^{-1})
Field observation #1	34.1	0.21	
Field observation #1 numerical simulation	34.1	0.21	0
Numerical simulation: vegetation temperature 5 °C lower than field observation #1	29.1	0.21	0
Numerical simulation: vegetation temperature 5 °C greater than field observation #1	39.1	0.21	0

Vegetation moisture is a very important parameter in fire propagation. It is present in the equation that describes the temperature of a fuel element in the condensed phase model (Eq. (A.9)) and in bulk density and specific heat contributions (Eqs. (A.10) and (A.11)). The higher the vegetation moisture, the higher the energy that must be supplied to its evaporation and the lower the speed at which the fire spreads.

5.6. Variation in vegetation surface area to volume ratio (SAV) for field observation #1 of Alta Floresta (MT)

In this section the simulations evaluate the effects of vegetation SAV varying 10% below and 10% above the SAV of field observation #1 of Alta Floresta (MT). For the case in which SAV is 10% lower than the value measured in field observation #1, simulated ROS is 0.195 m min^{-1}. For the case in which the variable is 10% higher, simulated ROS is 0.225 m min^{-1} (Table 12).

Vegetation SAV is an important variable in the characterization of vegetation. A low value for this variable indicates that for a given volume, the convective heat transfer (Eqs. (A.4) and (A.5)), radiation (Eqs. (A.6)–(A.8)), moisture evaporation (Eq. (A.14)) and combustible products volatilization (Eq. (A.15)) are smaller. Therefore, ROS decreases when the vegetation SAV decreases.

5.7. Variation in vegetation bulk density for field observation #1 of Alta Floresta (MT)

These simulations evaluated what would happen if the vegetation bulk density was 10% lower and 10% higher than actual value measured in field observation #1 of Alta Floresta (MT). In the case where the vegetation bulk density is 10% lower than the value measured in field observation #1, simulated ROS is 0.22 m min^{-1}. For the case in which the variable is 10% higher, simulated ROS is 0.20 m min^{-1} (Table 13).

Vegetation bulk density is also an important variable in vegetation characterization. A larger value for this variable indicates that for a given volume, there is proportionally more vegetation and less air, which makes fire propagation more difficult. If there is more vegetation there is proportionally more drag force (Eqs. (A.1)–(A.3)) and greater heat exchange by convection (Eqs. (A.4) and (A.5)). Radiation heat exchange is also affected (Eqs. (A.6)–(A.8)), as well as moisture evaporation (Eq. (A.14)) and combustible products volatilization (Eq. (A.15)). However, as can be seen in Table 13, ROS variation is not greatly influenced by vegetation bulk density when compared with the change in vegetation moisture (Table 11).

5.8. Summary of parameters variations for field observation #1 of Alta Floresta (MT)

ROS is the end result of all the physical processes of surface fire, under certain initial and boundary conditions. The comparison of the result of these processes, although it is of utmost practical interest, is difficult to be made conclusively.

Table 14 provides a summary of items (c) through (g) above. Vegetation moisture content, surface to volume ratio and bulk density are very important input parameters in WFDS.

As can be seen from Table 14, ROS variation because of vegetation moisture content (0.02 m min^{-1}) is twice the variation because of vegetation bulk density (0.01 m min^{-1}) for the same percentage change in each variable. Because of this, the next section presents a more detailed study on the vegetation moisture content.

5.9. Study on variation in vegetation moisture content for field observation #1 of Alta Floresta (MT)

In order to better understand the effects of the vegetation moisture content on ROS, two additional numerical simulations were done to evaluate what would happen if the vegetation moisture content were 20% lower and 20% higher than actual value measured in field observation #1 of Alta Floresta (MT). Table 15 shows data already presented in Table 11 plus the two additional numerical simulations.

Table 15 shows that the variation in ROS because of a change in the vegetation moisture content is linear for the range of plus/minus 20%, according to WFDS results.

Fig. 9 presents the numerically simulated mass loss time history for the vegetation in the domain for the original field observation and for the extreme vegetation moisture content variation cases. Curves for vegetation moisture content variation of plus/minus 10% are not shown, but they lie in between the original and the respective extreme case. As the vegetation bulk density remains the same as the numerical simulations refer to field

Table 11
Parametric variation in vegetation moisture for field observation #1.

	Vegetation moisture	ROS (m min^{-1})	Difference between simulated ROS and field observation ROS (m min^{-1})
Field observation #1	0.1438	0.21	
Field observation #1 numerical simulation	0.1438	0.21	0
Numerical simulation: vegetation moisture 10% lower than field observation #1	0.1294	0.23	0.02
Numerical simulation: vegetation moisture 10% greater than field observation #1	0.1582	0.19	−0.02

Table 12
Parametric variation in vegetation surface area to volume ratio (SAV) for field observation #1.

	Vegetation SAV (m^{-1})	ROS (m min^{-1})	Difference between simulated ROS and field observation ROS (m min^{-1})
Field observation #1		0.21	
Field observation #1 numerical simulation	4000	0.21	0
Numerical simulation: vegetation SAV 10% lower than field observation #1	3600	0.195	−0.015
Numerical simulation: vegetation SAV 10% greater than field observation #1	4400	0.225	0.015

observation #1 of Alta Floresta (MT) and the only change is the vegetation moisture content, the initial dry mass is the same. As already mentioned, an increase in vegetation moisture content causes a decrease in ROS. This slower fire propagation causes less vegetation to be burned in a period of time. In Fig. 9, after 180 s there was approximately three times more vegetation to burn in the case of higher vegetation moisture content than in the original case. It is also interesting to note the behavior of the mass loss rate curves in Fig. 10. The mass loss rate has its maximum when the fire front reaches the boundaries of computational domain, when the fire front circle has its maximum diameter. After that, vegetation burning continues to the corners of the numerical domain in a mass loss rate smaller that tends to zero. The curve for the case of higher vegetation moisture content does not reach its maximum until 180 s, which means that the fire front hadn't reach the boundaries of the numerical domain. The curves in Fig. 10 conform to the slopes of the curves in Fig. 9.

As before, time histories of the predicted radiant and convective heat fluxes refer to a grid cell located along the litter's surface 35 cm from its center. It can be seen from Figs. 11 and 12 that radiation heat flux is dominant over convection heat flux, independent of the amount of vegetation moisture content. The figures have the same scale for ease of comparison. Comparing the curves in Fig. 11, it can be seen that the fire front reaches the grid cell in analysis as faster as the lower the vegetation moisture content. It is interesting to observe the area under each curve of the radiation heat flux. It indicates the amount of net radiation received by the fuel element in the grid cell in analysis. For the curve representing the vegetation moisture content 20% lower than the original case, the area is 0.0255 kJ. For the original case the area is 0.0297 kJ and for the higher vegetation moisture content the area is 0.0310 kJ. However, the increase in this net energy received by the fuel element is not linear with the increase in vegetation moisture content. The energy increases 17% from the lower vegetation moisture content case to the original case, while it increases only 4% from the original case to the higher vegetation moisture content case. The analysis of the convective heat flux curves of Fig. 12 is even more interesting. It can be seen from Fig. 12 that in the early stages of the convective heat transfer, the fuel element under analysis provides heat to the surrounding air. This happens because the fire indraft air comes from outside the fire perimeter, as indicated in Fig. 13. This fresh air is heated by the fuel element that received energy by radiation. There are then two areas to be considered for each curve, one negative in which the fuel element provides energy by convection to the surrounding air and the other positive, in which the fuel element receives energy by convection because of the hot gases from combustion or the preheated air inside the litter and closer to the fire front. The negative area in the graphs for the lower vegetation moisture content case, the original case and the higher vegetation moisture content case are 0.0019, 0.0027 and 0.0034 kJ respectively. The positive areas considering the same sequence of cases are 0.0079, 0.0084 and 0.0096 kJ respectively. The net energy received by the fuel element because of convection is then 0.0060, 0.0057 and 0.0062 kJ respectively. It is surprising the net energy received by the fuel element in the original case to be smaller than the net energy received in the lower vegetation moisture content case. This is explained by the proportion of the energy provided and the energy received. In the first case it is 33% while in the second it is 25% only. Nonetheless, the net energy received by the fuel element by radiation is 4.3 times the net energy received by convection in the case where the vegetation moisture content is 20% lower, 5.2 times in the original case and 5.0 times in the higher vegetation moisture content case.

5.10. Analysis on ROS calculation by the numerical model and conservation equations non-linearity

The numerical model conservation equations are strongly non-linear and therefore it is not to be expected, a priori, the trend showed by the sensitivity analysis when more than one parameter varies at the same time. The sensitivity analysis was performed varying only one parameter at a time, while the others were kept constant. In this section, it is analyzed the impact on ROS because of a change in more than one parameter at the same time. The surface to volume ratio was kept constant in all numerical simulations and it was shown that the fuel moisture content and the fuel bulk density have the highest impact on ROS.

Table 16 presents a comparison between each two numerical simulations in order to assess how the fuel moisture content and the fuel combustible material bulk density influences the ROS. This was done in order to evaluate the conservation equations non-linearity impact on ROS calculation. The fourth column in Table 16 represents the joint variation of the fuel moisture content and the

Table 13
Parametric variation in bulk density for field observation #1.

	Bulk density (kg m^{-3})	ROS (m min^{-1})	Difference between simulated ROS and field observation ROS (m min^{-1})
Field observation #1	13.34	0.21	
Field observation #1 numerical simulation	13.34	0.21	0
Numerical simulation: bulk density 10% lower than field observation #1	12.01	0.22	0.01
Numerical simulation: bulk density 10% greater than field observation #1	14.67	0.20	−0.01

Table 14
Summary of parametric variation for field observation #1 of Alta Floresta (MT).

	Simulated ROS – field observation ROS (m min^{-1})				
	Air humidity (%)	Vegetation temperature (°C)	Vegetation moisture	Vegetation SAV (m^{-1})	Vegetation bulk density (kg m^{-3})
Field observation #1 numerical simulation	0	0	0	0	0
Numerical simulation: parameter lower than field observation #1	0	0	0.02	−0.015	0.01
Numerical simulation: parameter greater than field observation #1	0	0	−0.02	0.015	−0.01

combustible material bulk density. As shown in Table 14, the impact on ROS because of the fuel moisture content is twice the impact on ROS because of the combustible material bulk density. This column then presents the amount of change in the fuel moisture content multiplied by two plus the amount of change in the combustible material bulk density. This is a linear relationship and it does not represent the actual calculation performed by the numerical model to determine the ROS. The comparison between this column with the numerically calculated ROS variation (fifth column) shows the effects of the conservation equations non-linearity.

As an increase in both fuel moisture content and fuel bulk density decreases ROS, a positive value in the fourth column of Table 16 represents a decrease in ROS variation in the fifth column of Table 16. Likewise, a negative value in the fourth column of Table 16 represents a decrease in ROS variation. Although there is a correlation between the fourth and fifth columns in Table 16, it is not linear.

6. Conclusions

A physics-based, transient, three-dimensional, coupled fire–atmosphere numerical model for simulating fire spread through surface fuels on flat terrain was used and tested against measurements from crude by design burn field observations in the Brazilian Amazon forest litter.

Most of the ROS results from the numerical simulation are in the range measured in field observations or very close to them. The reasons for the deviations can be various, including the non-homogeneity in the field observation, measurement errors, number of field measurements and limitations of the numerical model. The lack of the measurement uncertainty of the experimental data and the fact that there are not enough data in order to evaluate the propagation of the measurement errors makes it difficult, if not impossible, to investigate the source of the discrepancy between the experimental and numerical ROS results.

In the range of parameter variation considered, the simulations showed that the important parameters for the model are the vegetation moisture content, surface area to volume ratio and bulk density. According to the results of numerical simulations, vegetation moisture content is the most important variable in the surface fire propagation. As the absorption coefficient by radiation is a direct function of the vegetation bulk density and surface area to volume ratio, these parameters affect the numerical behavior of the surface fire. The vegetation initial temperature and air humidity in the range of variation studied did not influence the fire rate of spread. The simulations also showed that the radiation process is very important and directly affects all other processes and the rate of propagation. Convection is less important because of the absence of external wind.

In the next field observations, measurements of the convective and radiative heat fluxes need to be recorded to compare with the

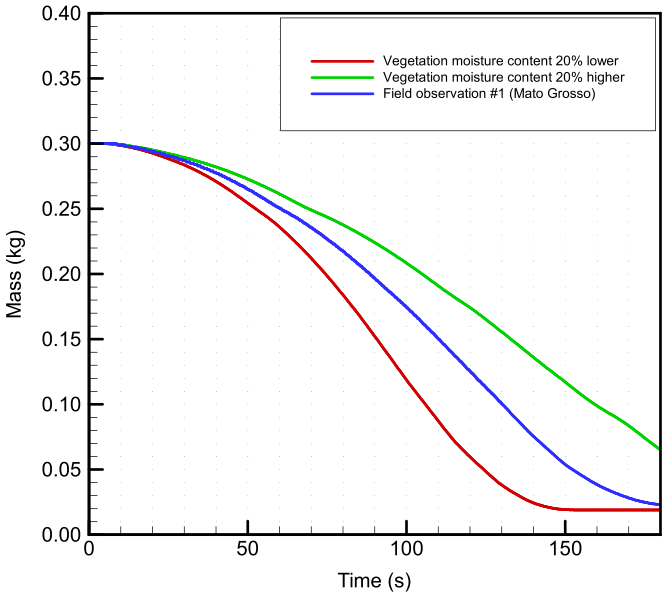

Fig. 9. Mass loss time history curves for vegetation moisture content analysis.

Table 15
Variation in vegetation moisture for field observation #1.

	Vegetation moisture	ROS (m min^{-1})	Difference between simulated ROS and field observation ROS (m min^{-1})
Field observation #1	0.1438	0.21	
Field observation #1 numerical simulation	0.1438	0.21	0
Numerical simulation: vegetation moisture 20% lower than field observation #1	0.1150	0.25	0.04
Numerical simulation: vegetation moisture 10% lower than field observation #1	0.1294	0.23	0.02
Numerical simulation: vegetation moisture 10% greater than field observation #1	0.1582	0.19	−0.02
Numerical simulation: vegetation moisture 20% greater than field observation #1	0.1726	0.17	−0.04

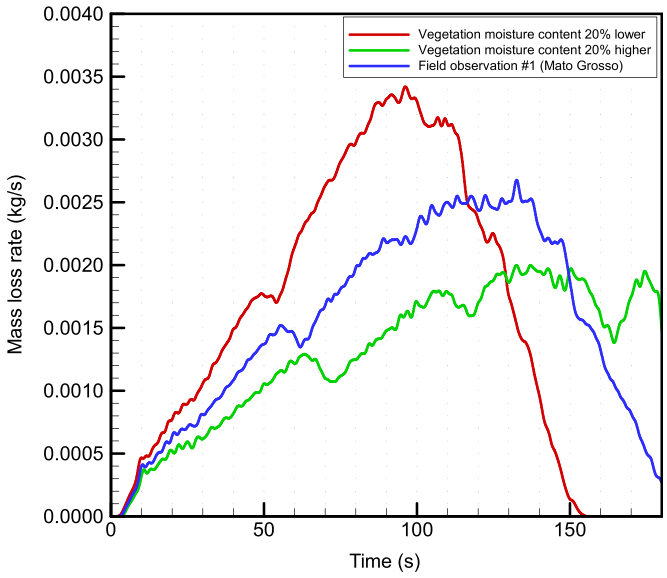

Fig. 10. Mass loss rate time history curves for vegetation moisture content analysis.

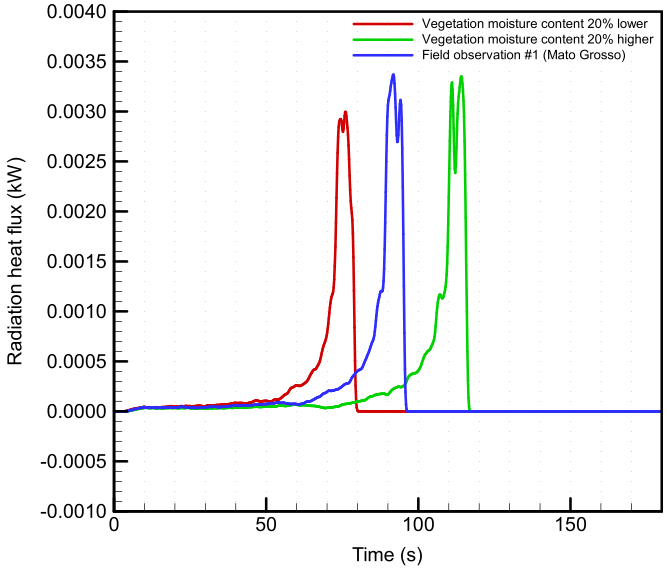

Fig. 11. Time history curves of the predicted radiant heat flux in a grid cell located along the litter's surface 0.35 m from the center of the surface fire for vegetation moisture content analysis.

values from the simulations. Another future line of investigation will be on the physical parameters of the vegetation that are relevant to radiative and convective heat transfer, such as the absorption coefficient and soot fraction.

Acknowledgments

Partial funding for this work was received under Grant # 2008/04490-4 and 2011/20679-2, São Paulo Research Foundation (FAPESP).

Appendix A

This appendix presents the equations necessary for understanding the model behavior as described in Mell *et al.* [9].

The drag force per unit volume $\langle \mathbf{f}_D''' \rangle_{V_b}$ represents the momentum removed from the gas by the vegetation. Explicit filtering of the discrete drag sources gives

$$\left\langle f_D''' \right\rangle_{V_b} = \beta_e \sigma_e \frac{3}{8} C_{D,e} \bar{\rho} |u_e - \tilde{u}| (u_e - \tilde{u}) \tag{A.1}$$

where the subscript e denotes a fuel type. The 3/8 factor has also

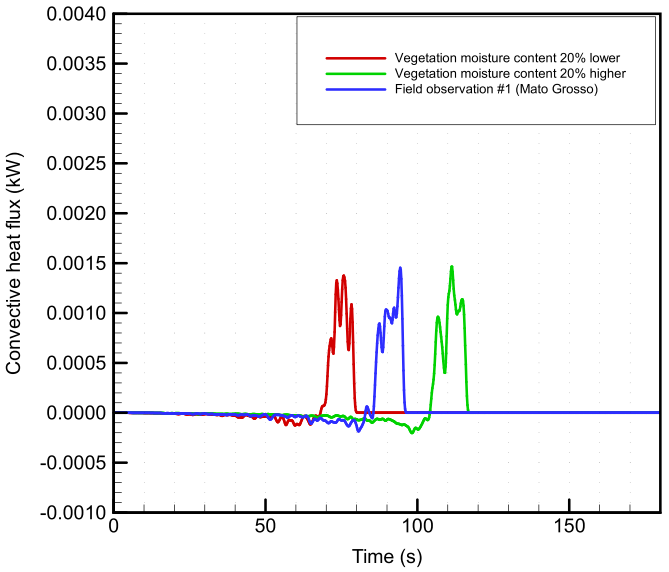

Fig. 12. Time history curves of the predicted convective heat flux in a grid cell located along the litter's surface 0.35 m from the center of the surface fire for vegetation moisture content analysis.

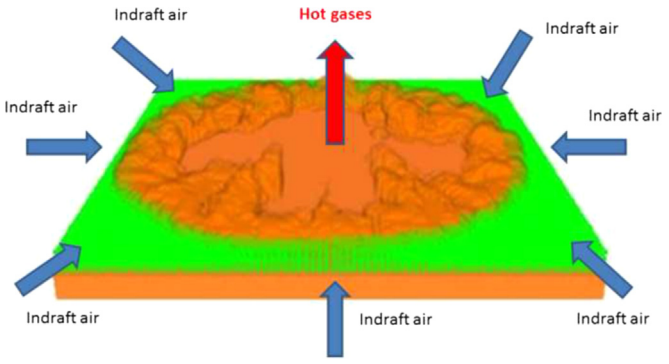

Fig. 13. Air indraft for fire front.

Table 16
Qualitative assessment of ROS variation (field observation × numerical simulation).

Field observation	Vegetation moisture (% variation)	Combustible material bulk density (% variation)	Moisture / Bulk density combined parameter (% variation)	Numerical ROS variation (% variation)
ALTA FLORESTA (MT)				
#1 and #3	−3	29	22	−5
#1 and #4	14	−2	26	−14
#3 and #4	18	−24	12	−10
CRUZEIRO DO SUL (AC)				
#1 and #4	120	13	253	−39
#1 and #6	30	6	66	−17
#1 and #8	60	−7	112	−26
#4 and #6	−41	−6	−88	36
#4 and #8	−27	−17	−72	21
#6 and #8	23	−12	33	−11

been used in numerical simulations of flame spread through a forest fuel bed [8], Mediterranean shrubs [3], and Australian grassland fires [4]. This factor is 1/8 for a spherical fuel element, and was also used by Porterie et al. [22] and Porterie et al. [23]. The value of the drag coefficient C_D depends on the local Reynolds number Re_e

$$C_{D,e}=\begin{cases}24/Re_e, & Re_e \le 1\\ 24\left(0.85+0.15\,Re_e^{0.687}\right)/Re_e, & 1 < Re_e < 1000\\ 0.44, & 1000 \le Re_e\end{cases} \tag{A.2}$$

$$Re_e=\frac{2\rho|u_e-\tilde{u}|r_e}{\tilde{\mu}} \tag{A.3}$$

where re is the equivalent radius for a sphere $r_e=3/\sigma_e$ and σ_e is the surface-to-volume ratio for fuel elements of type e. Similar expressions for $C_{D,e}$ have been used previously [9,22,23].

The convective heat transfer between the condensed and gaseous phases is [9]

$$\left\langle q'''_{c,b}\right\rangle_{V_b}=\beta_e\sigma_e h_{c,e}\left(T_e-\tilde{T}\right) \tag{A.4}$$

The surface-to-volume ratio for fuel elements of type e that is shown in Eq. (A.4) is not zero only when there is a condensed phase in the computational cell. The empirical correlation for the convective heat transfer coefficient is [22]

$$h_{c,e}=0.5k\left(\tilde{T}\right)\frac{0,683\,Re_e^{0.466}}{2/\sigma_e} \tag{A.5}$$

where the Reynolds number is based on the relation $\sigma=2/r$ for cylinders of radius r.

Fires from vegetative fuels are soot-laden. Since the radiation spectrum of soot is continuous, it is assumed that the gas behaves as a spectrally independent or gray medium. This results in a significant reduction in computational expense. The vegetative fuel is assumed to be comprised of fixed, uniformly distributed within the bulk volume V_b, non-scattering, perfectly absorbing, subgrid fuel elements.

Following Consalvi et al. [24], for simplicity the fuel element is assumed to be spherical. The absorption coefficient is,

$$\kappa_{b,e}=\frac{1}{4}\frac{\rho_{bv,e}}{\rho_e}\sigma_e=\frac{1}{4}\beta_e\sigma_e \tag{A.6}$$

This expression for the absorption coefficient has been used in other fire spread models [3,4,8,9] and has been experimentally validated for vegetative fuels [25]. The final form of the radiation transfer equation (RTE) is then given by

$$\hat{\mathbf{s}}\cdot\nabla I\left(\mathbf{x},\hat{\mathbf{s}}\right)=\kappa\left[I_b\left(\tilde{T}\right)-I\left(\mathbf{x},\hat{\mathbf{s}}\right)\right]+\kappa_{b,e}\left[I_b\left(T_e\right)-I\left(\mathbf{x},\hat{\mathbf{s}}\right)\right] \tag{A.7}$$

A table containing the values of κ as a function of species mass fractions and temperature for a given mixture of participating gaseous species (H_2O and CO_2) and soot particulate is computed before the simulation begins. A soot evolution model is not used. Instead, the mass of soot generated locally is an assumed fraction (χ_s) of the mass of fuel gas consumed by the combustion process. In the WFDS simulations reported here, χ_s=0.01 is used. Values of χ_s for Douglas fir range from less than 0.01–0.025 under flaming conditions [26]. No paper was found in the literature referencing values of χ_s for litter fires in Amazon. Integrating the RTE (A.7) over all solid angles gives the equation for conservation of radiant energy,

$$\begin{aligned}\nabla\cdot\tilde{\mathbf{q}}_r(\mathbf{x})&=\kappa\left[4\pi I_b\left(\tilde{T}\right)-\bar{U}(\mathbf{x})\right]+\kappa_{b,e}\left[4\pi I_b\left(T_e\right)-\bar{U}(\mathbf{x})\right]\\&=\kappa\left[4\pi I_b\left(\tilde{T}\right)-\bar{U}(\mathbf{x})\right]+\langle\nabla\cdot\mathbf{q}_{r,b}\rangle_{V_b}\end{aligned} \tag{A.8}$$

where $\bar{U}$ is the integrated radiation intensity.

The model for the thermal degradation of a thermally thin vegetative fuel used here is similar to that employed by others (e.g., [22]) and previously in WFDS simulations of fire spread in grassland fuels [4] and Douglas fir [9]. The equation governing the temperature of a thermally thin fuel element k with the explicit spatial filters applied is

$$\begin{aligned}\rho_{e,b}c_{p,e}\frac{dT_e}{dt}=&-\Delta h_{vap}\left\langle m'''_{b,H_2O}\right\rangle_{V_b}-\Delta h_{pyr}\\&\left\langle m'''_{b,F}\right\rangle_{V_b}-\left\langle q'''_{c,b}\right\rangle_{V_b}-\left\langle\nabla\cdot\mathbf{q}_{r,b}\right\rangle_{V_b}\end{aligned} \tag{A.9}$$

The third and fourth terms on the right-hand-side of Eq. (A.9) are the fuel element bulk contributions from unresolved convection and radiative heat transfer, which are given by Eqs. (A.4) and (A.8).

In the condensed phase model, the bulk density and specific heat have contributions from dry virgin vegetative fuel and moisture,

$$\rho_{e,b}=\rho_{b,v}+\rho_{b,H_2O} \tag{A.10}$$

$$c_{p,e}=\frac{\rho_{b,v}c_{p,v}+\rho_{b,H_2O}c_{p,H_2O}}{\rho_b} \tag{A.11}$$

where initially $\rho_{e,b,H_2O}=M_e\rho_{b,v}$ and M_e is the fuel moisture content of vegetative element type e and it is represented as a fraction, not a percent.

The temperature Eq. (A.9) for the fuel bed is solved assuming a two-stage endothermic decomposition process: water evaporation followed by vegetative fuel volatilization. This results in a mass loss of vegetative fuel:

$$\frac{d\rho_{e,b}}{dt}=\left\langle m'''_{e,b}\right\rangle_{V_b}=\left\langle m'''_{b,H_2O}\right\rangle_{V_b}+\left\langle m'''_{b,F}\right\rangle_{V_b} \tag{A.12}$$

with the net heat flux divergence defined as

$$\left\langle q'''_{net}\right\rangle_{V_b}\equiv-\left\langle q'''_{c,b}\right\rangle_{V_b}-\left\langle\nabla\cdot\mathbf{q}_{r,b}\right\rangle_{V_b} \tag{A.13}$$

The moisture evaporation model used here is

$$\begin{aligned}\left\langle m'''_{e,b,H_2O}\right\rangle_{V_b}&=\beta_e m'''_{e,H_2O}\\&=\begin{cases}0, & T_e<100°C\\ \dfrac{\left\langle q'''_{net}\right\rangle_{V_b}}{\Delta h_{vap}}, & T_e=100°C,\ \rho_{H_2O}V_b>0,\ \left\langle q'''_{net}\right\rangle_{V_b}>0\end{cases}\end{aligned} \tag{A.14}$$

and the thermal degradation model is represented as

$$\begin{aligned}\left\langle m'''_{e,b,F}\right\rangle_{V_b}&=\beta_e m'''_{e,F}\\&=\begin{cases}0, & T_e<127°C\\ \dfrac{\left\langle q'''_{net}\right\rangle_{V_b}}{\Delta h_{pyr}}\left(\dfrac{T_e-127}{100}\right), & 127°C\le T_e\le 227°C,\\ \dfrac{\left\langle q'''_{net}\right\rangle_{V_b}}{\Delta h_{pyr}}, & T_e\ge 227°C\\ \text{for all cases,} & \rho_{b,F}V_b>\chi_{e,residue}\rho_{bv}V_b,\ \left\langle q''_{net}\right\rangle_{V_b}>0\end{cases}\end{aligned} \tag{A.15}$$

where $\chi_{e,residue}$ is the residue fraction for fuel elements of type e. The heat of vaporization for water is Δh_{vap}=2259 kJ kg^{-1} and the

heat of pyrolysis is Δh_{pyr}=416 kJ kg^{-1} [3]. The initial temperature $T_e(t_0)$ is ambient or user defined.

The temperature of the vegetative fuel evolves according to Eq. (A.9), which was also used (up to the point of pyrolysis) by Albini [27,28]. Once T_e reaches the boiling temperature it is assumed that drying requires all of the available heat so that T_e=100 °C until all the moisture has evaporated. After all the moisture has been removed, the temperature of the fuel element evolves according to Eq. (A.9) with $\langle \dot{m}_{b,H_2O} \rangle_{V_b}$=0. With a net influx of heat, T_e continues to rise, eventually reaching a temperature T_e=127 °C , when pyrolysis begins. The model for moisture evaporation and fuel thermal degradation uses the temperature dependent mass loss rate expression of Morvan and Dupuy [3]. The fuel volatilization model is based on thermogravimetric analysis of a number of vegetation species [29,30]. Since residue oxidation is not modeled, smoldering or glowing combustion is not accounted for.

Appendix B

Nomenclature used in this paper

Variable	Description units
C_D	Drag coefficient [−]
c_p	Specific heat at constant pressure kJkg^{-1}K^{-1}
D^*	Characteristic diameter of the fire m
$\mathbf{f}_D'''$	Drag force per unit volume kg m^{-2} s^{-2}
h	Mixture enthalpy kJ kg^{-1}
$I(\mathbf{x}, \hat{\mathbf{s}})$	Radiation intensity W m^{-2}
$I_b(\mathbf{x}, \hat{\mathbf{s}})$	Blackbody radiation intensity W m^{-2}
k	Thermal conductivity W m^{-1} K^{-1}
$m_{b,i}'''$	Bulk mass source density for gas species i due to thermal degradation of vegetation kg m^{-3} s^{-1}
m_b'''	Bulk mass source due to thermal degradation of vegetation kg m^{-3} s^{-1}
q_{net}'''	Convective plus radiative heat source kW m^{-3}
q	Heat flux vector kW m^{-2}
$\dot{q}'''$	Heat release rate per unit volume kW m^{-3}
r	Radius m
Re	Reynolds number [−]
$\hat{\mathbf{s}}$	Unit vector in direction of radiation intensity [−]
t	Tempo s
T	Temperature °C
u	Velocity vector m s^{-1}
U	Integrated radiation intensity W m^{-2}
V_b	Volume of the computational cell m^3
x	Position vector m
β	Packing ratio [−]
Δh_{pyr}	Heat of pyrolysis kJ kg^{-1}
Δh_{vap}	heat of vaporization kJ kg^{-1}
κ	Radiative absorption coefficient [−]
μ	Dynamic viscosity of the gaseous mixture kg m^{-1} s^{-1}
ρ	Mass density kg m^{-3}
σ_e	Surface-to-volume ratio for fuel elements of type e m^{-1}
$\chi_{residue}$	Fraction of virgin vegetative fuel converted to residue [−]

Subscripts

b	Bulk vegetative fuel quantity or blackbody
c	Convective, combustion, chemical
D	Drag
e	Fuel element type
F	Fuel species
r	Radiative
v	Virgin dry vegetation

References

[1] P.A. Santoni, A. Simeoni, J.L. Rossi, F. Bosseur, F. Morandini, X. Silvani, J.H. Balbi, D. Cancellieri, L. Rossi, Instrumentation of wildland fire: characterisation of a fire spreading through a Mediterranean shrub, Fire Saf. J. 41 (2006) 171–184.
[2] F. Morandini, X. Silvani, L. Rossi, P.A. Santoni, A. Simeoni, J.H. Balbi, J.L. Rossi, T. Marcelli, Fire spread experiment across Mediterranean shrub: influence of wind on flame front properties, Fire Saf. J. 41 (2006) 229–235.
[3] D. Morvan, J.L. Dupuy, Modeling the propagation of a wildfire through a Mediterranean shrub using a multiphase formulation, Combust. Flame 138 (2004) 199–210.
[4] W.E. Mell, M.A. Jenkins, J. Gould, P. Cheney, A physics based approach to modeling grassland fires, Int. J. Wildland Fire 16 (2007) 1–22.
[5] D. Morvan, S. Méradji, G. Accary, Physical modelling of fire spread in Grasslands, Fire Saf. J. 44 (2009) 50–61.
[6] F. Plourde, S. Doan-Kim, J.C. Dumas, J.C. Malet, A new model of wildland fire simulation, Fire Saf. J. 29 (1997) 283–299.
[7] V. Novozhilov, B. Moghtaderi, D.F. Fletcher, J.H. Kent, Computational fluid dynamics modelling of wood combustion, Fire Saf. J. 27 (1996) 69–84.
[8] D. Morvan, J.L. Dupuy, Modeling fire spread through a forest fuel bed using a multiphase formulation, Combust. Flame 127 (2001) 1981–1984.
[9] W.E. Mell, A. Maranghides, R. McDermott, S. Manzello, Numerical simulation and experiments of burning Douglas fir trees, Combust. Flame 156 (2009) 2023–2041.
[10] R.G. Silva, Manual de prevenção e combate aos incêndios florestais, Instituto Brasileiro do Meio Ambiente e dos Recursos Naturais Renováveis, Brasília, 1998.
[11] M.A. Cochrane, Fire science for rainforests, Nature 421 (2003) 913–919.
[12] J.A. Carvalho, C.A.G. Veras, E.C. Alvarado, E.C. Sandberg, E.R. Carvalho, R. Gielow, J.C. Santos, Fire spread around a forest clearing site in the Brazilian amazon region, International Wildland Fire Ecology and Fire Management Congress, 2003.
[13] WFDS, Web page for the WFDS model, 2013. ⟨http://www.fs.fed.us/pnw/fera/research/wfds/index.shtml⟩.
[14] J.W. Deardorff, Stratocumulus-capped mixed layers derived from a three-dimensional model, Bound.-Layer Meteorol. 18 (1980) 495–527.
[15] R.W. MacCormack, The Effect of Viscosity in Hypervelocity Impact Cratering, AIAA Paper,1969, pp. 69–354.
[16] B.F. Magnussen, B.H. Hjertager, On mathematical modeling of turbulent combustion with special emphasis on soot formation and combustion, Proc. Combust. Inst. 16 (1976) 719–729.
[17] R.C. Rothermel, A mathematical model for predicting fire spread in wildland fuels, USDA Forest Service, Intermountain Forest and Range Experiment Station 1972, Research Paper RP-INT-115, Ogden, UT.
[18] M.S. Jayalakshmy, J. Philip, Thermophysical properties of plant leaves and their influence on the environment temperature, Int. J. Thermophys. 31 (2010) 2295–2304.
[19] R.A. Susott, Characterization of the thermal properties of forest fuels by combustible gas analysis, For. Sci. 28 (2) (1982) 404–420.
[20] K.B. McGrattan, S. Hostikka, J. Floyd, W.E. Mell, R. McDermott, Fire Dynamics Simulator Technical Reference Guide, Mathematical Model, vol. 1, Technical Report NISTIR Special Publication, 1018-5, National Institute of Standards and Technology, Gaithersburg, Maryland, 2012.
[21] X. Silvani, F. Morandini, Fire spread experiments in the field: temperature and heat fluxes measurements, Fire Saf. J. 44 (2009) 279–285.
[22] B. Porterie, D. Morvan, M. Larini, J.C. Loraud, Wildfire propagation: a two dimensional multiphase approach, Combust. Explos. Shock Waves 34 (2) (1998) 139–150.
[23] B. Porterie, D. Morvan, J.C. Loraud, M. Larini, Firespread through fuel beds: modeling of wind-aided fires and induced hydrodynamics, Phys. Fluids 12 (7) (2000) 1762–1782.
[24] J.L. Consalvi, B. Porterie, J.C. Loraud, Model of radiative heat transfer in particulate medium, Int. J. Heat Mass Transf. 45 (2002) 2755–2768.
[25] B.W. Butler, in: Proceedings of the12th Conference of Fire and Forest Meteorology, 1993, p. 26.
[26] C.P. Bankston, B.T. Zinn, R.F. Browner, E.A. Powell, Aspects of the mechanisms of smoke generation by burning materials, Combust. Flame 41 (1981) 273–292.
[27] F.A. Albini, A model for fire spread in wildland fuels by radiation, Combust. Sci. Technol. 42 (1985) 229–258.
[28] F.A. Albini, Wildland fire spread by radiation – a model including fuel cooling by natural convection, Combust. Sci. Technol. 45 (1986) 101–113.
[29] A.P. Dimitrakipoulos, Pyric properties of some dominant Mediterranean vegetation species, J. Anal. Appl. Pyrol. 60 (2001) 123.
[30] C. Moro, Technical Report, INRA Equipe de Prédes Incendies de Forêt, 1997.